Single-beam shaper-based pulse characterization and compression using MIIPS sonogram

Dmitry Pestov, Vadim V. Lozovoy, and Marcos Dantus*

Department of Chemistry, Michigan State University, East Lansing, Michigan 48824, USA
**Corresponding author: dantus@msu.edu*

Received January 6, 2010; revised March 9, 2010; accepted March 17, 2010;
posted March 22, 2010 (Doc. ID 122380); published April 28, 2010

A single-beam pulse-shaper-based sonogram technique for spectrometer-free measurement and compensation of laser pulse phase distortions is demonstrated. Phase and amplitude shaping is used to both generate an internal reference and scan the time delay between waveforms corresponding to isolated spectral bands of the input spectrum, thereby directly reconstructing the first derivative of the spectral phase. The accuracy and precision of the approach are evaluated by measuring the group delay introduced by transmission through water or reflection from a broadband dielectric mirror. © 2010 Optical Society of America

OCIS codes: 320.5520, 320.5540, 320.7160.

Pulse characterization and the ability to deliver predefined optical waveforms to a target location are the cornerstones of ultrafast optics and its applications. The shorter the pulses, the broader their bandwidth and the more they are prone to group-delay dispersion (GDD). To satisfy ever increasing requirements toward pulse characterization and compression, traditional autocorrelation measurements have been replaced in the past decade by more advanced pulse characterization techniques [1,2]. Advances in pulse shaping technology have led to the implementation of evolutionary algorithms for pulse compression [3,4], shaper-assisted versions of frequency-resolved optical gating [5], spectral phase interferometry for direct electric field construction [6], and the spectrally and temporally resolved upconversion technique (STRUT) [5,7]. The paradigm of integrated pulse characterization and compression was realized with the development of the multiphoton intrapulse interference phase scan (MIIPS) [8].

MIIPS is a self-referenced pulse characterization method that takes advantage of a calibrated pulse shaper to measure the unknown spectral phase. The spectrally resolved nonlinear signal, generated by the shaped pulses, is recorded as a function of a single scan parameter. The acquired series of spectra yield an accurate measurement of the spectral phase function $\varphi(\omega)$ through an analytical formula. The approach does not rely on an evolutionary algorithm. Given that the method incorporates a pulse shaper, it is possible to compensate for phase distortions and to cycle the measurement and compression steps a few times to achieve unprecedented accuracy [9].

In this Letter, we extend the MIIPS concept by having the spectrometer function delegated to the pulse shaper as well. We use spectral amplitude modulation (transmission $T=0$ or $T=1$) to isolate two narrow spectral bands at a time [Fig. 1(a)]. The time overlap between the corresponding waveforms is obtained by measuring a nonlinear optical response and looking for constructive interference. Assuming that the phase distortions within the narrow band can be approximated by a linear function, only the slope (time delay) needs to be adjusted to find the maximum nonlinear signal. We encode a linear phase function, $\varphi_{\text{delay}}=\tau\cdot(\omega-\omega_{\text{slit}})$, with variable time delay τ across one of the spectral bands. The offset of the carrier frequency ω by the center frequency of the band, ω_{slit}, allows performing intensity cross correlation (XC) of the collinearly propagating pulses (τ scan). The delay values corresponding to the maxima of the XC traces map out the first derivative of the compensation phase mask, $\varphi_c'(\omega)$. Once one of the transmission slits (T-slits) has been scanned over the spectral frequency range, the first derivative of the compensation phase can be interpolated across the entire spectrum. Its direct integration over frequency

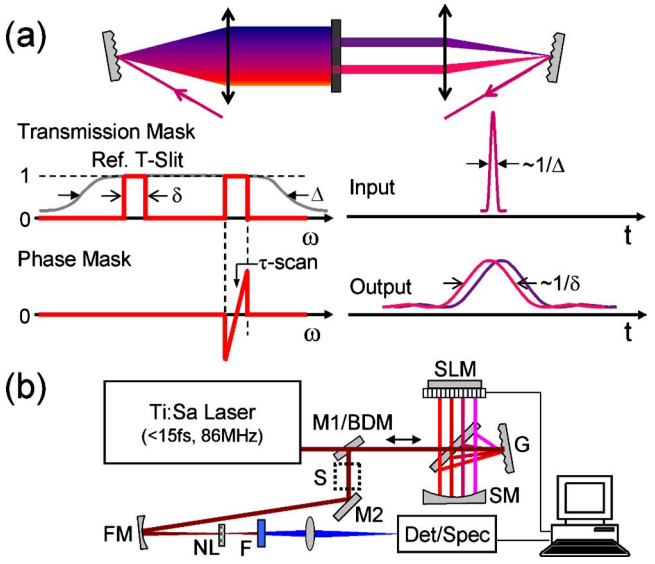

Fig. 1. (Color online) (a) Principle of the MIPS-S technique. Amplitude shaping is used to select two narrow bands of width δ within the input laser spectrum of width $\Delta(\delta \ll \Delta)$. The corresponding waveforms are cross correlated at the target location by using phase shaping, and the relative group delay between the two selected spectral bands is measured. (b) Experimental setup layout. G, grating; SM, spherical mirror ($f=500$ mm), SLM, spatial light modulator; M1-2, steering mirrors, BDM, broadband dielectric mirror; S, sample; FM, focusing mirror ($f=250$ mm); NL, nonlinear crystal; F, filter; Det/Spec, spectrometer.

ω gives the pulse spectral phase $\varphi(\omega)$, which is equal to $-\varphi_c(\omega)$. We abbreviate this sonogram-like implementation of MIIPS as MIIPS-S.

Sonogram measurements of ultrashort laser pulses were first reported by Fork *et al.* [10], where amplified 50 fs pulses were cross correlated with different spectral bands of a broadband continuum. The technique was evaluated more thoroughly by Chilla and Martinez [11], and since then has been implemented in a variety of experimental geometries [7,12,13]. Most of them rely on upconversion in a nonlinear crystal and are known as variants of STRUT [7,13]. One common disadvantage of all those schemes is the need for a reference beam. Second, compensation of phase distortions therein is delegated to other elements of the setup, being a simple prism-pair compressor, specially designed dielectric mirrors, or a pulse shaper. MIIPS-S uses an internal reference and supports the all-in-one approach to measurement and compensation of phase distortions. We believe it also compares favorably with the recently reported shaper-assisted version of STRUT [5].

The layout of the experimental setup is shown schematically in Fig. 1(b). We used a Ti:sapphire laser oscillator (KM Labs) and a folded 4*f* pulse shaper with a dual-mask, one-dimensional, 640 pixel spatial light modulator (CRi SLM-640-D). The output laser beam was sent through a quartz cuvette (Precision Cells) with distilled water or bounced off a broadband dielectric mirror (BDM). It was then focused on a ~20-μm-thick KDP crystal. The second-harmonic generation (SHG) signal was separated from the IR light by a 3-mm-thick BG39 glass filter, refocused into a fiber-coupled spectrometer (Ocean Optics USB4000), and spectrally integrated; i.e., the spectrometer functioned as a single-channel detector.

Amplitude modulation was used here to create the T-slits; however, polarization and/or phase shaping can also be used to mitigate the nonlinear contribution from the rest of the spectrum. The T-slits were chosen to be 31 pixels wide (~10 nm or 0.03 rad/fs at 800 nm). One fixed spectral region near the center was designated the reference, and the other was shifted across the SLM pixel array after every τ scan. The two T-slits were offset spectrally by at least one width to avoid distortions of XC traces by the interference between intraband and interband contributions into the SHG signal. The XC traces were fitted with a Gaussian function to deduce the relative time delay. Note that even though a single reference T-slit can be used for MIIPS-S, we found it advantageous to assign different reference T-slits for $\varphi_c'(\omega)$ reconstruction in the red and blue parts of the spectrum [Fig. 2(a)], and then to overlay the two curves by using common experimental points.

A single MIIPS-S measurement and compression restored a pulse with significant nonlinear GDD and resulted in SHG intensity of >80% of the maximum, expected for a transform-limited (TL) pulse. Two or three additional measurement–compensation cycles (~5 min each) boosted the SHG intensity to the 97%–100% level. The SHG spectra and spectrally integrated SHG signal, recorded for six consecutive correction cycles are shown in Fig. 2(b). The data indicate that three cycles are sufficient to compress the pulse down to TL within the noise limit. The resulting profile for $\varphi_c'(\omega)$ is shown in Fig. 2(c). The error bars obtained for three consecutive measurements of $\varphi_c'(\omega)$ and denoted Err$[\varphi_c'(\omega)]$ are shown in the bottom of Fig. 2(c) and give an average error of ±2.5 fs over $1/e^2$ bandwidth. The compensation phase $\varphi_c(\omega)$ and estimated errors are given in Fig. 2(d).

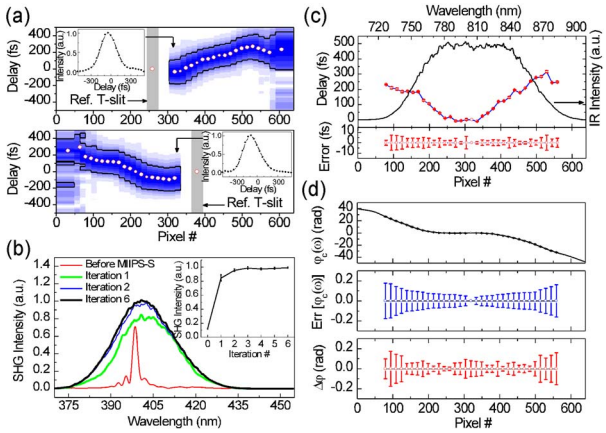

Fig. 2. (Color online) (a) Normalized XC data acquired during the first iteration of MIIPS-S. The T-slits for both spectral bands, fixed and scanned, are 31 pixel wide, except at the edges. The circles show the positions of XC maxima. The black outline marks the half-maximum level for the normalized XC traces. The insets are examples of obtained XC traces. (b) SHG spectra, recorded for zero phase on the SLM and selected compensation masks after MIIPS-S. The inset shows the dependence of spectrally integrated SHG signal on the number of measurement–compensation iterations. (c) Typical laser spectrum and $\varphi_c'(\omega)$ profile obtained via MIIPS-S. The panel at the bottom highlights the precision error for the time delay, estimated from three MIIPS-S measurements. (d) The top panel shows the compensation phase obtained by direct integration of $\varphi_c'(\omega)$ from (c). The center panel gives the estimated phase error, accumulated through the integration of experimental $\varphi_c'(\omega)$ data. The bottom panel highlights the incremental phase uncertainty $\Delta\varphi$ over a single T-slit. The last quantity is a product of $\varphi_c'(\omega)$ error and the T-slit spectral bandwidth δ.

The accuracy and precision of MIIPS-S were determined by measuring the GDD acquired by a pulse transmitted through distilled water and comparing our results with those in the literature. The experimental $\varphi'(\omega)$ data for two different nominal path lengths are presented in Fig. 3. They are in good agreement with the fit data from Coello *et al.* [9], plotted as solid curves. The error bars show the precision for two consecutive measurements, ±3.5 fs within $1/e^2$ bandwidth of the laser spectrum. Deviation from the solid curves indicates the measurement accuracy and is limited by shaper calibration and phase distortion precompensation errors. The average accuracy within $1/e^2$ bandwidth was estimated to be ±7 fs. The second-order polynomial fit of our data gives the group-velocity dispersion of 24.04±0.46 fs^2/mm and the third-order dispersion of 44.8±8.2 fs^3/mm at 800 nm. From Sellmeier's formula in [9], one obtains 24.90 fs^2/mm and 33.05 fs^3/mm.

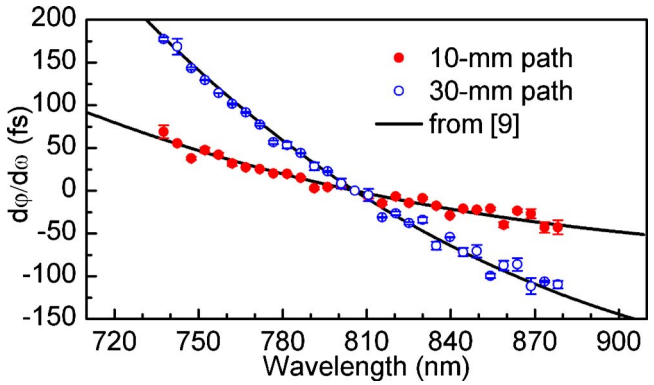

Fig. 3. (Color online) MIIPS-S dispersion measurements on distilled water for 10 and 30 mm nominal path lengths. Every scan consists of four measurement–compensation iterations, starting from the phase compensation mask obtained with an empty cuvette. Other scan parameters are the same as in Fig. 2. The group delay is taken to be zero at 805.8 nm (SLM pixel 319).

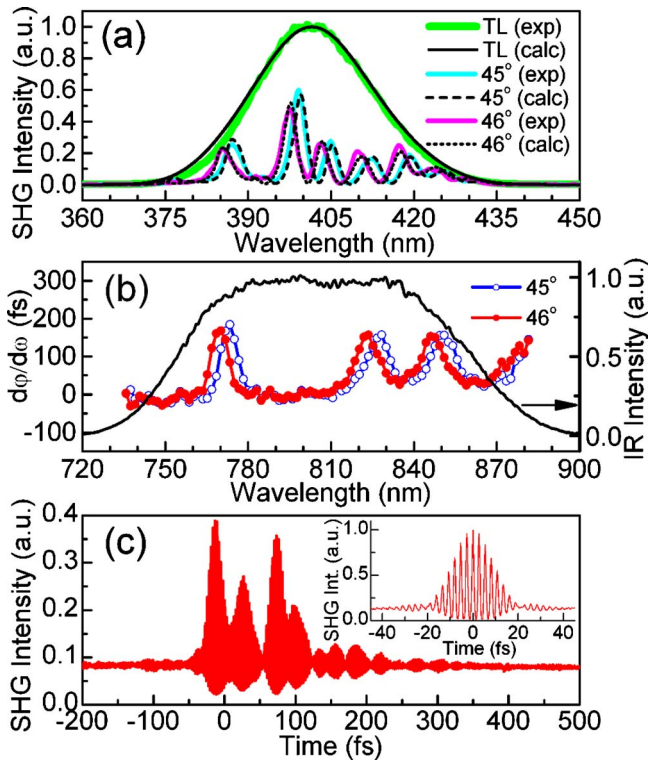

Fig. 4. (Color online) Measurement and compensation of phase distortions introduced by a BDM. (a) Experimental and simulated SHG spectra produced by initially TL pulses after a single bounce off the BDM set at 45° and 46° incidence angles. The experimental SHG spectrum for a TL pulse is obtained after MIIPS-S compensation of phase distortions for the 45° incident beam. (b) Group-delay spectra measured for the two incidence angles. The black solid curve maps the laser spectrum. (c) Interferometric XC of the pulse after the BDM for 45° incidence. Inset, interferometric cross correlation of the pulse after compensation of phase distortions from the BDM.

We have tested different BDMs by using MIIPS-S. The most striking results were obtained for a New Focus NIR5102 mirror, having a pair of multilayer high-reflectance coatings, and are highlighted in Fig. 4. MIIPS-S measurements for 45° and 46° incidence angles reveal several distinct GDD oscillations, where the group delay changes rapidly by as much as 150 fs. These features are known to be the result of Gires–Tournois interference between reflections coming from different layers of the mirror [14]. The peaks in the SHG spectra [Fig. 4(a)] correlate with the GDD oscillations in Fig. 4(b) if one accounts for double- and sum-frequency processes. The waveform profile after one bounce of a TL pulse off the mirror, obtained using multiple independent comb shaping technique [15] and shown in Fig. 4(c), reveals severe distortions introduced by the BDM. The interferometric autocorrelation of the laser pulse after MIIPS-S compensation [the inset of Fig. 4(c)] confirms that the pulse after the BDM was recompressed properly.

In conclusion, we described a pulse-shaper-based sonogram method for pulse characterization and compression. MIIPS-S does not require an external reference and allows for spectrometer-free retrieval of the first derivative of the spectral phase. This method is ideally suited for conditions in which it is difficult to acquire a spectrum but easy to obtain an integrated nonlinear optical signal, e.g., in nonlinear optical microscopy or when the laser pulses propagate long distances in open air or fibers.

References

1. R. Trebino, *Frequency Resolved Optical Gating* (Springer, 2002).
2. C. Iaconis and I. A. Walmsley, Opt. Lett. **23**, 792 (1998).
3. T. Baumert, T. Brixner, V. Seyfried, M. Strehle, and G. Gerber, Appl. Phys. B **65**, 779 (1997).
4. D. Meshulach, D. Yelin, and Y. Silberberg, J. Opt. Soc. Am. B **15**, 1615 (1998).
5. A. Galler and T. Feurer, Appl. Phys. B **90**, 427 (2008).
6. B. von Vacano, T. Buckup, and M. Motzkus, Opt. Lett. **31**, 1154 (2006).
7. T. K. Rhee, T. S. Sosnowski, T. B. Norris, J. A. Arns, and W. S. Colburn, Opt. Lett. **19**, 1550 (1994).
8. V. V. Lozovoy, I. Pastirk, and M. Dantus, Opt. Lett. **29**, 775 (2004).
9. Y. Coello, B. W. Xu, T. L. Miller, V. V. Lozovoy, and M. Dantus, Appl. Opt. **46**, 8394 (2007).
10. R. L. Fork, C. H. B. Cruz, P. C. Becker, and C. V. Shank, Opt. Lett. **12**, 483 (1987).
11. J. L. A. Chilla and O. E. Martinez, Opt. Lett. **16**, 39 (1991).
12. J. P. Foing, J. P. Likforman, M. Joffre, and A. Migus, IEEE J. Quantum Electron. **28**, 2285 (1992).
13. J. K. Rhee, T. S. Sosnowski, A. C. Tien, and T. B. Norris, J. Opt. Soc. Am. B **13**, 1780 (1996).
14. N. Matuschek, F. X. Kartner, and U. Keller, IEEE J. Sel. Top. Quantum Electron. **4**, 197 (1998).
15. D. Pestov, V. V. Lozovoy, and M. Dantus, Opt. Express **17**, 14351 (2009).